Supplement of Hydrol. Earth Syst. Sci., 29, 3833–3852, 2025
https://doi.org/10.5194/hess-29-3833-2025-supplement

Hydrology and Earth System Sciences
Open Access
EGU

Supplement of

An efficient hybrid downscaling framework to estimate high-resolution river hydrodynamics

Zeli Tan et al.

Correspondence to: Zeli Tan (zeli.tan@pnnl.gov)

Table S1. Gauge information.

Gauge #	USGS ID	Longitude	Latitude
1	08072300	-95.8069	29.7433
2	08072350	-95.7672	29.7230
3	08072470	-95.6432	29.7694
4	08072520	-95.7096	29.8051
5	08072600	-95.6869	29.8308
6	08072680	-95.6466	29.8672
7	08072700	-95.6258	29.8358
8	08072730	-95.6239	29.7903
9	08072760	-95.6058	29.7619
10	08072800	-95.5577	29.7622
11	08073100	-95.5236	29.7469
12	08073500	-95.4086	29.7602
13	08073600	-95.4805	29.8708
14	08073700	-95.4880	29.8513
15	08074000	-95.4694	29.8280
16	08074020	-95.3972	29.7752
17	08074150	-95.3681	29.7928
18	08074250	-95.3585	29.7666
19	08074500	-95.291	29.7494

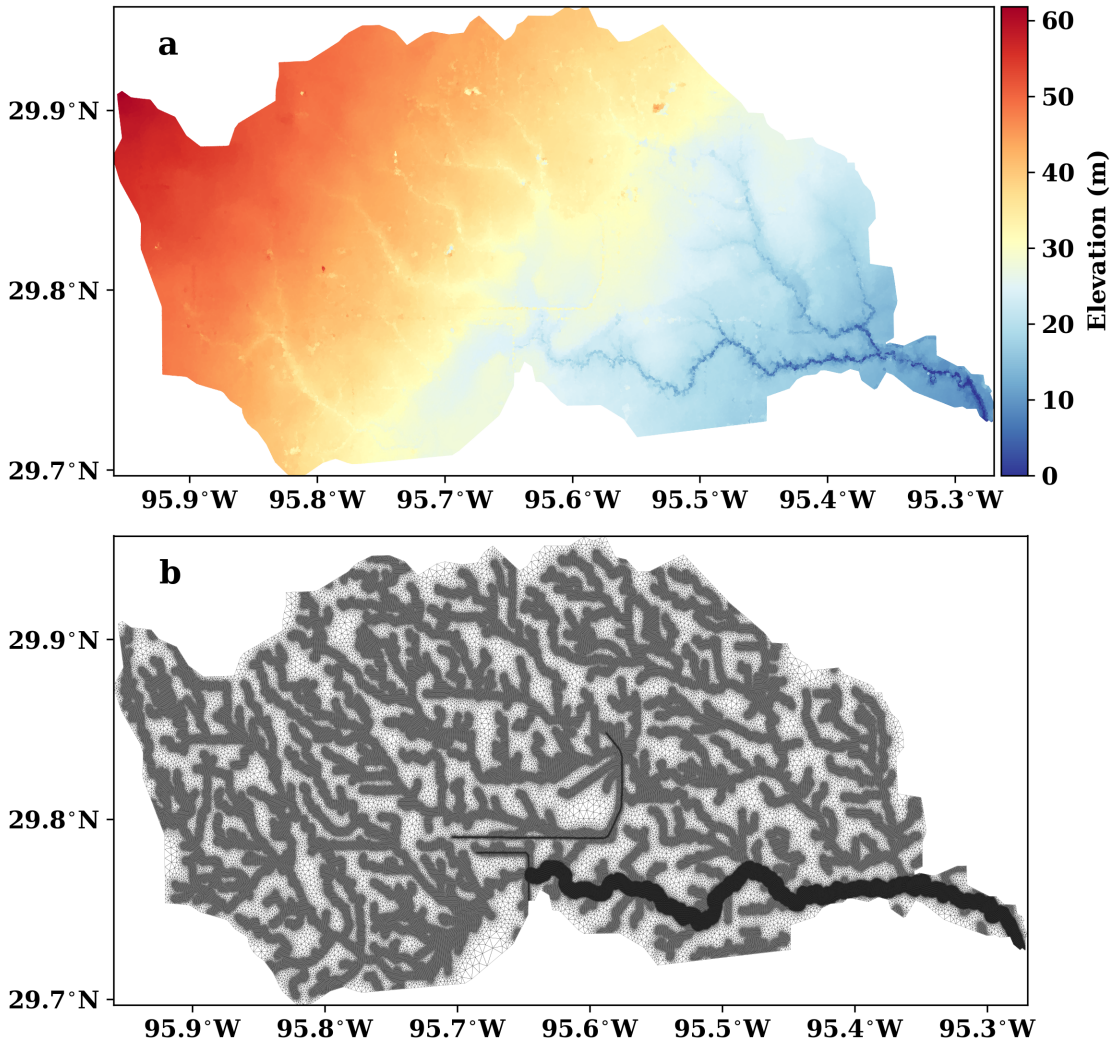

Figure S1. Topography data (a) used for the fine resolution mesh (b).

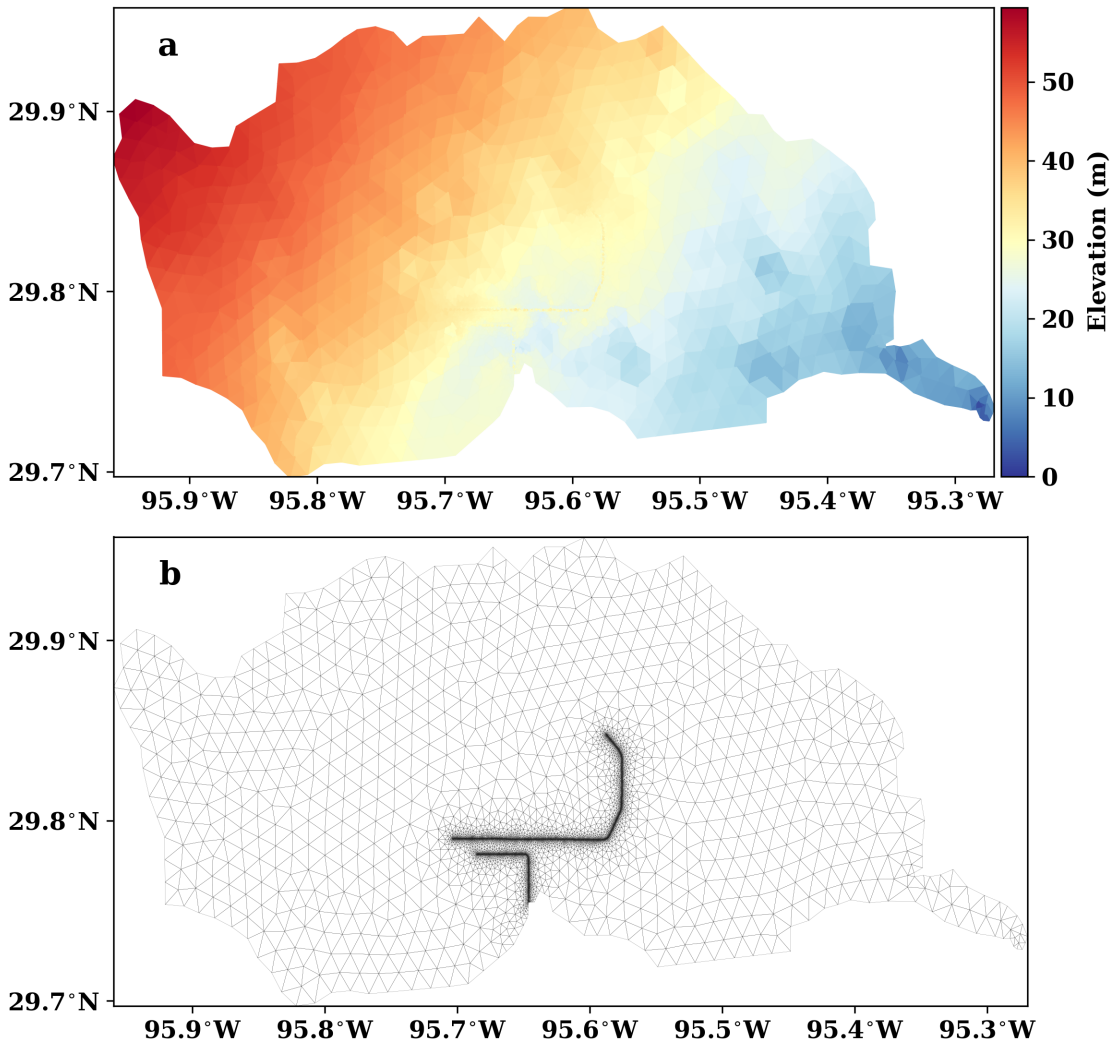

Figure S2. Topography data (a) used for the coarse resolution mesh (b).

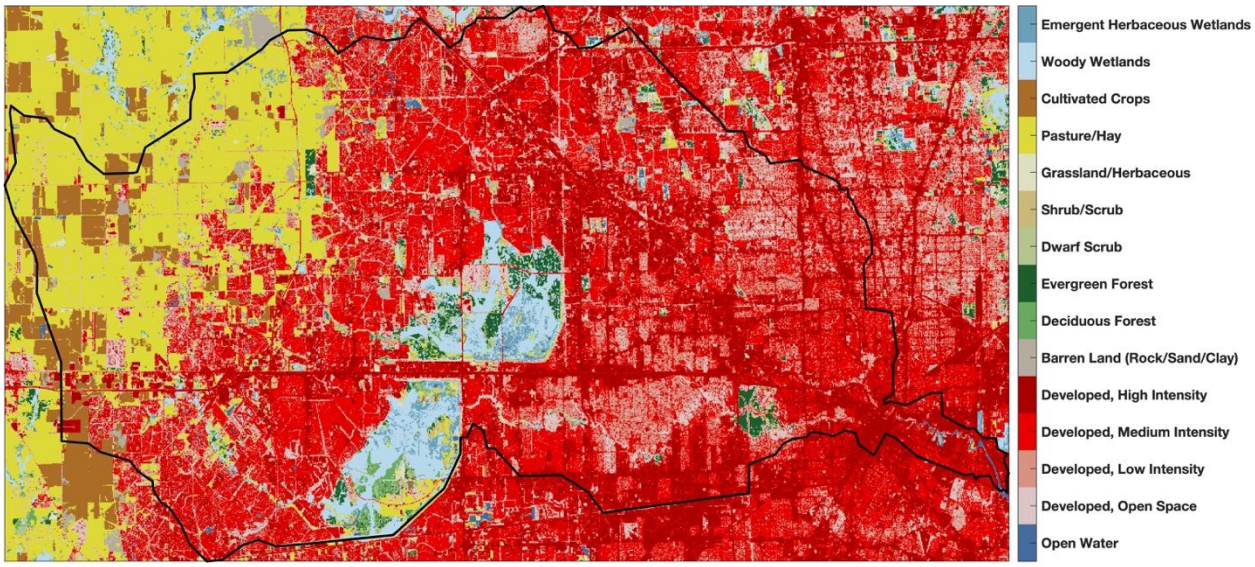

Figure S3. National Land Cover Dataset for the study domain. The black line delineates the watershed boundary.

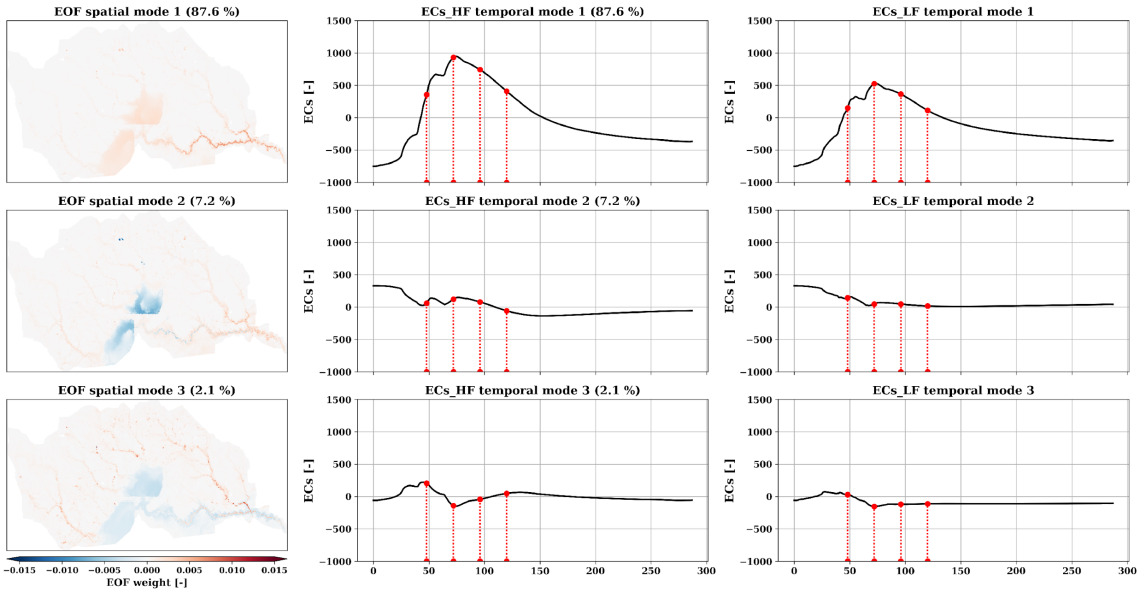

Figure S4. The first three EOF spatial modes (first column) and the corresponding ECs temporal modes of the high-fidelity (second column) and low-fidelity (third column) flow depth simulations for the Harvey flood event. The proportion of variance explained by the specific modes is shown in parentheses. Red dashed lines and dots indicate the timesteps at the 48th, 72th, 96th, and 120th hour time steps of the simulations. Blank grid cells in the maps of EOF spatial modes are dry grid cells.

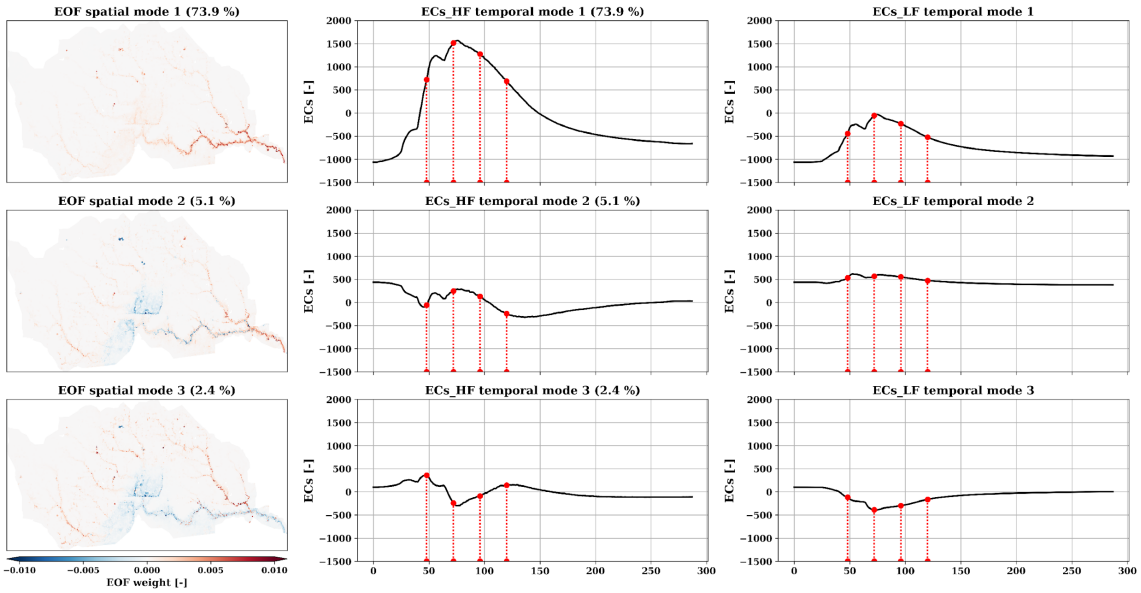

Figure S5. The first three EOF spatial modes (first column) and the corresponding ECs temporal modes of the high-fidelity (second column) and low-fidelity (third column) flow velocity simulations for the Harvey flood event. The proportion of variance explained by the specific modes is shown in parentheses. Red dashed lines and dots indicate the timesteps at the 48th, 72th, 96th, and 120th hour time steps of the simulations. Blank grid cells in the maps of EOF spatial modes are dry grid cells.

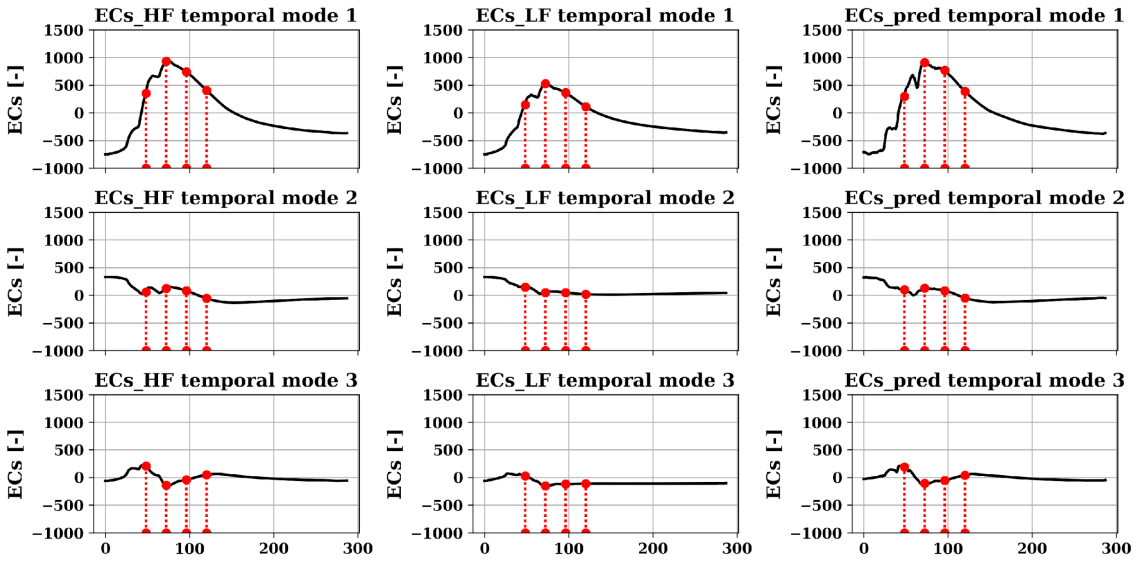

Figure S6. The first three ECs temporal modes of the high-fidelity (first column) and low-fidelity (second column) flow depth simulations, and the predicted first three ECs temporal modes for flow depth downscaling (third column) for the Harvey flood event. Red dashed lines and dots indicate the timesteps at the 48th, 72th, 96th, and 120th hour time steps of the simulations.

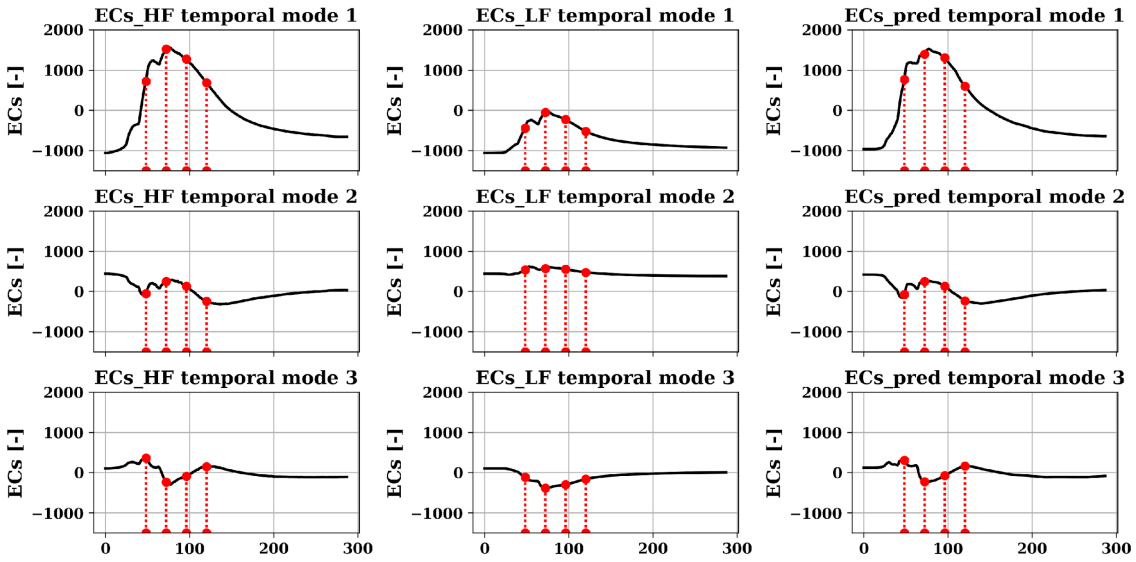

Figure S7. The first three ECs temporal modes of the high-fidelity (first column) and low-fidelity (second column) flow velocity simulations, and the predicted first three ECs temporal modes for flow velocity downscaling (third column) for the Harvey flood event. Red dashed lines and dots indicate the timesteps at the 48th, 72th, 96th, and 120th hour time steps of the simulations.

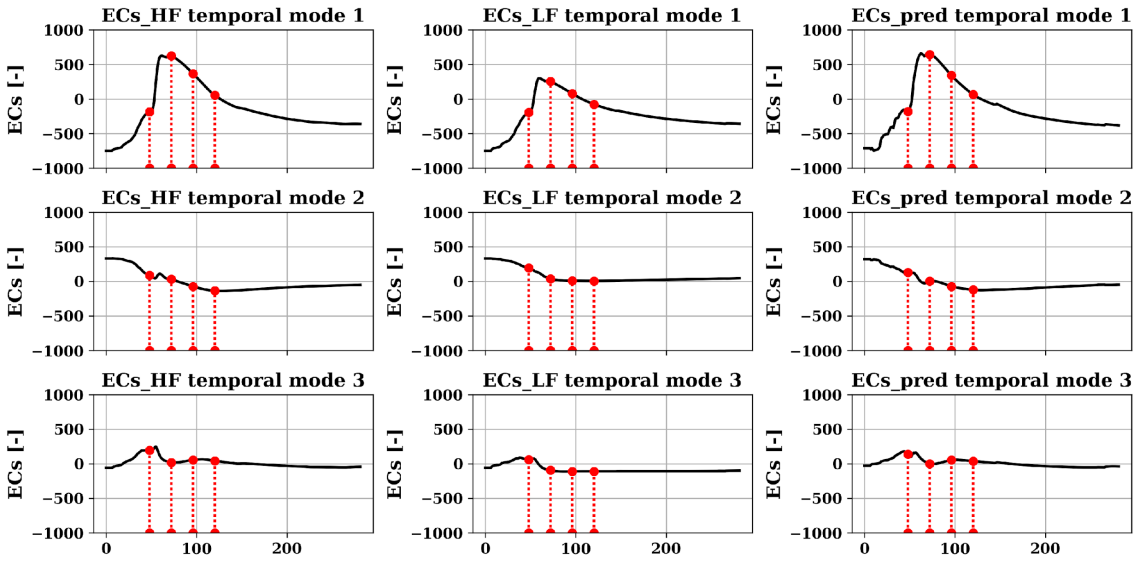

Figure S8. The first three ECs temporal modes of the high-fidelity (first column) and low-fidelity (second column) flow depth simulations, and the predicted first three ECs temporal modes for flow depth downscaling (third column) for the PGW flood event. Red dashed lines and dots indicate the 48th, 72th, 96th, and 120th hour time steps of the simulations.

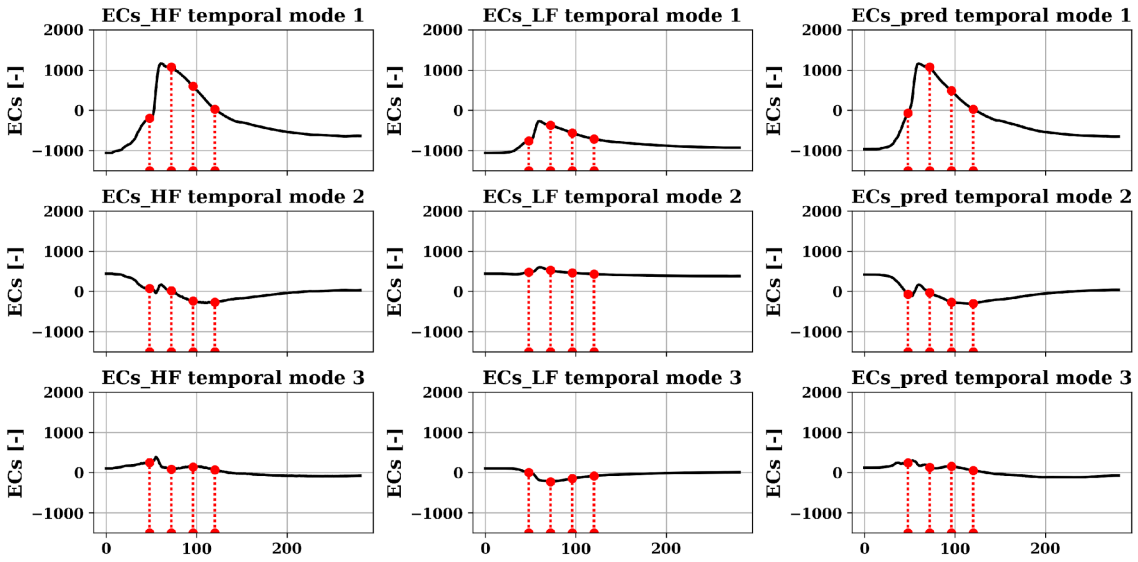

Figure S9. The first three ECs temporal modes of the high-fidelity (first column) and low-fidelity (second column) flow velocity simulations, and the predicted first three ECs temporal modes for flow velocity downscaling (third column) for the PGW flood event. Red dashed lines and dots indicate the 48th, 72th, 96th, and 120th hour time steps of the simulations.

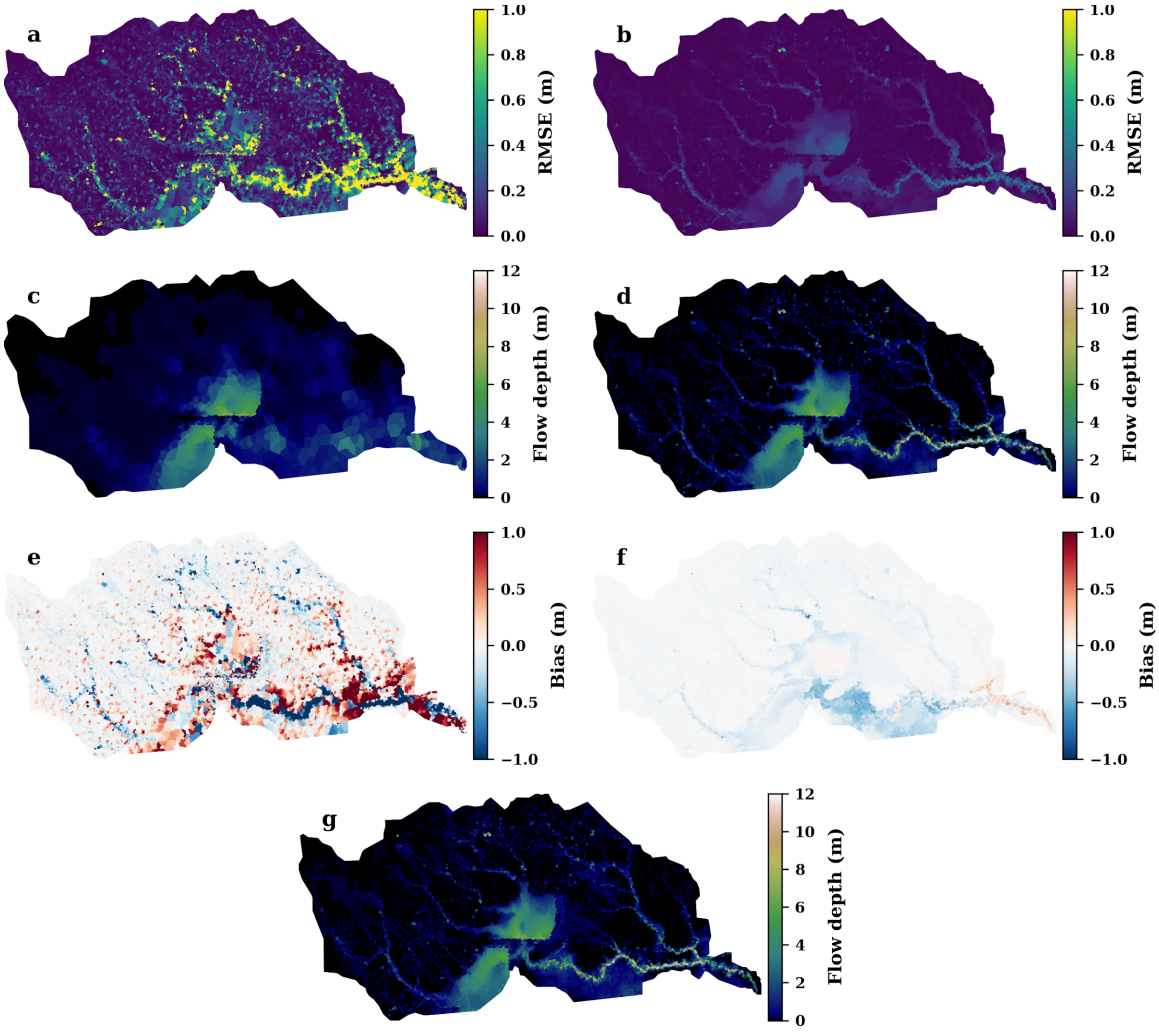

Figure S10. RMSE of simulated flow depth of the low-fidelity (a) and downscaled model (b) for the Harvey flood event, simulated flow depth of the low-fidelity (c) and downscaled model (d) at 01:00 am August 27, bias of the low-fidelity (e) and downscaled model (f) simulations at the timestep, and simulated flow depth of the high-fidelity model (g) at the timestep. RMSE and bias are calculated based on the difference between the low-fidelity or downscaled simulation and the high-fidelity simulation.

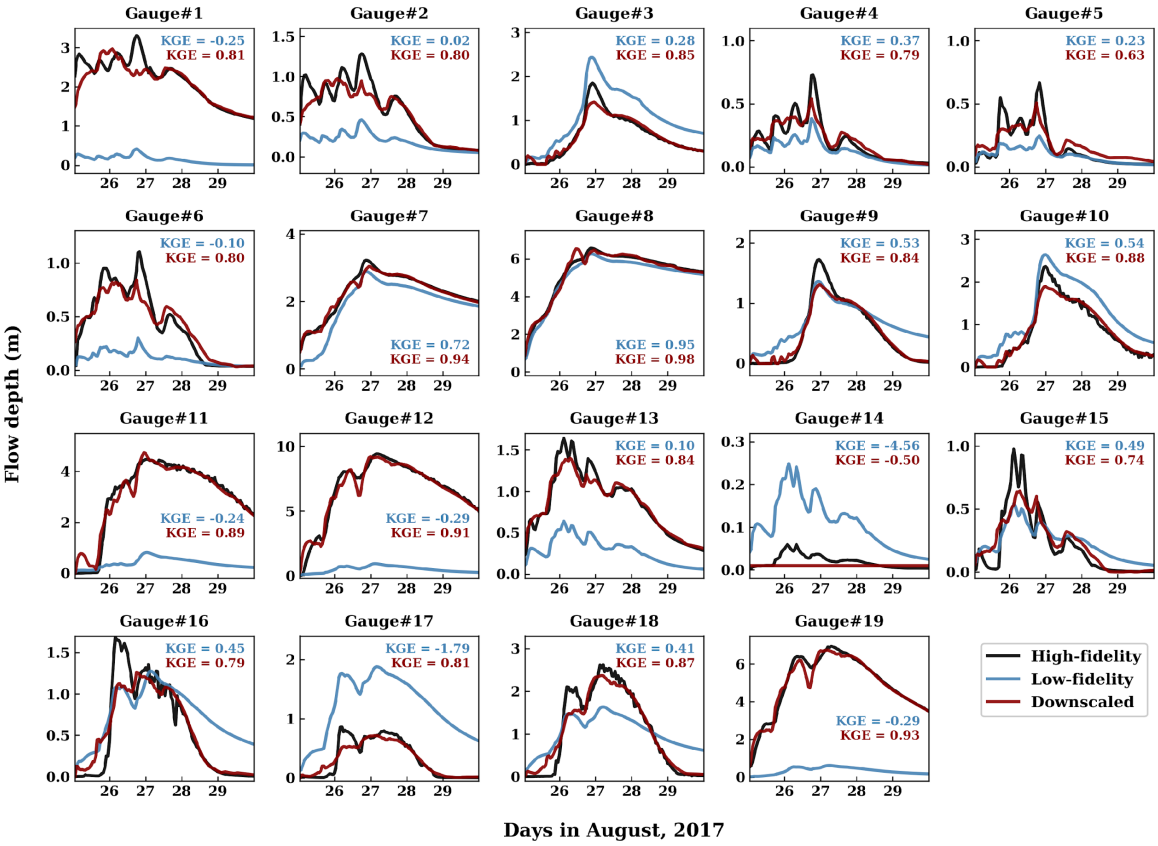

Figure S11. Comparison of the simulated flow depth of the high-fidelity model, the low-fidelity model, and the downscaled model at the selected USGS gauges (see Table S1 and Figure 2b) during the Harvey flood event.

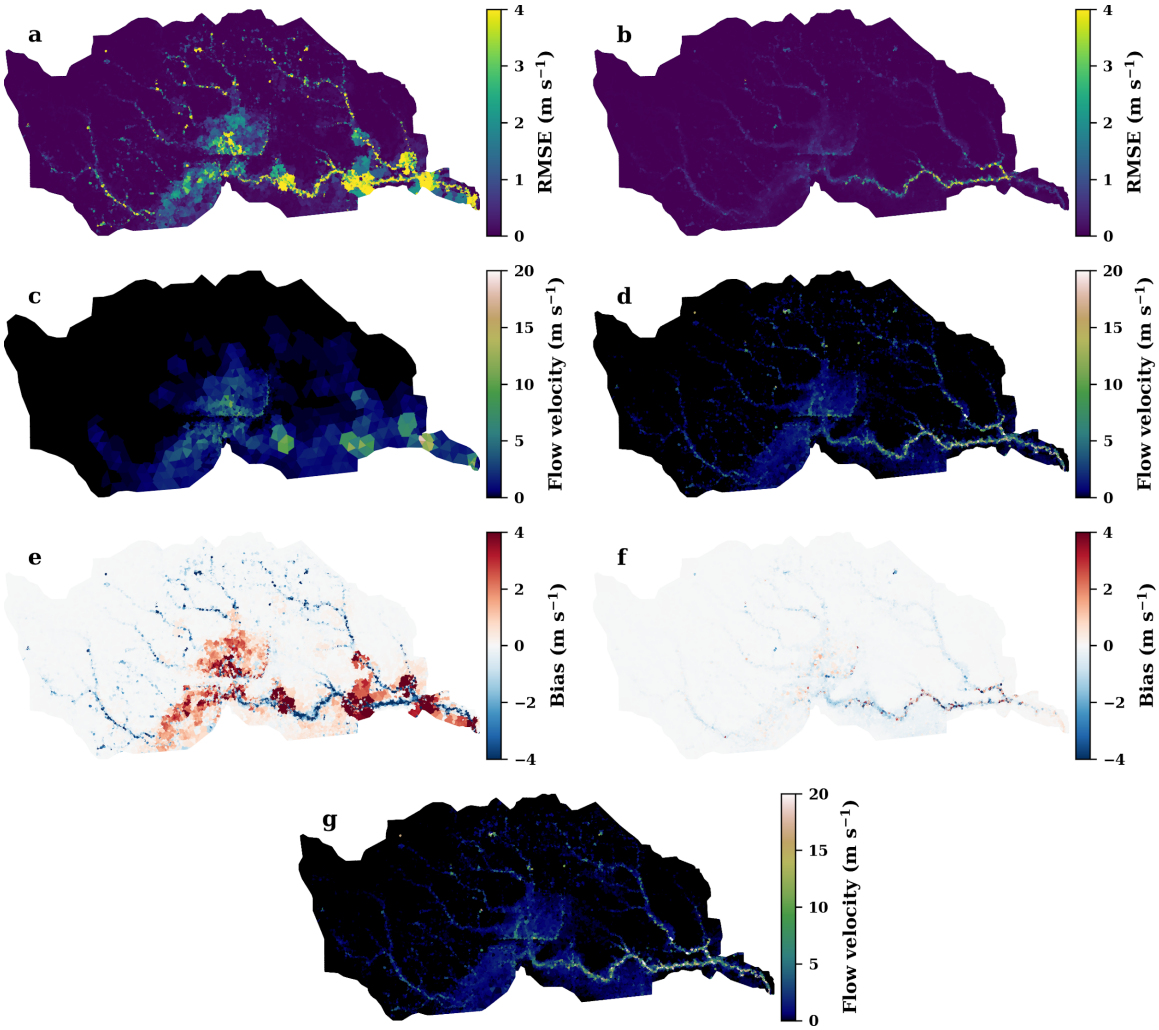

Figure S12. RMSE of the simulated flow velocity of the low-fidelity (a) and downscaled model (b) for the Harvey flood event, simulated flow velocity of the low-fidelity (c) and downscaled model (d) at 01:00 am August 27, bias of the low-fidelity model (e) and downscaled model (f) simulations at the timestep, and simulated flow velocity of the high-fidelity model (g) at the timestep. RMSE and bias are calculated based on the difference between the low-fidelity or downscaled simulation and the high-fidelity simulation.

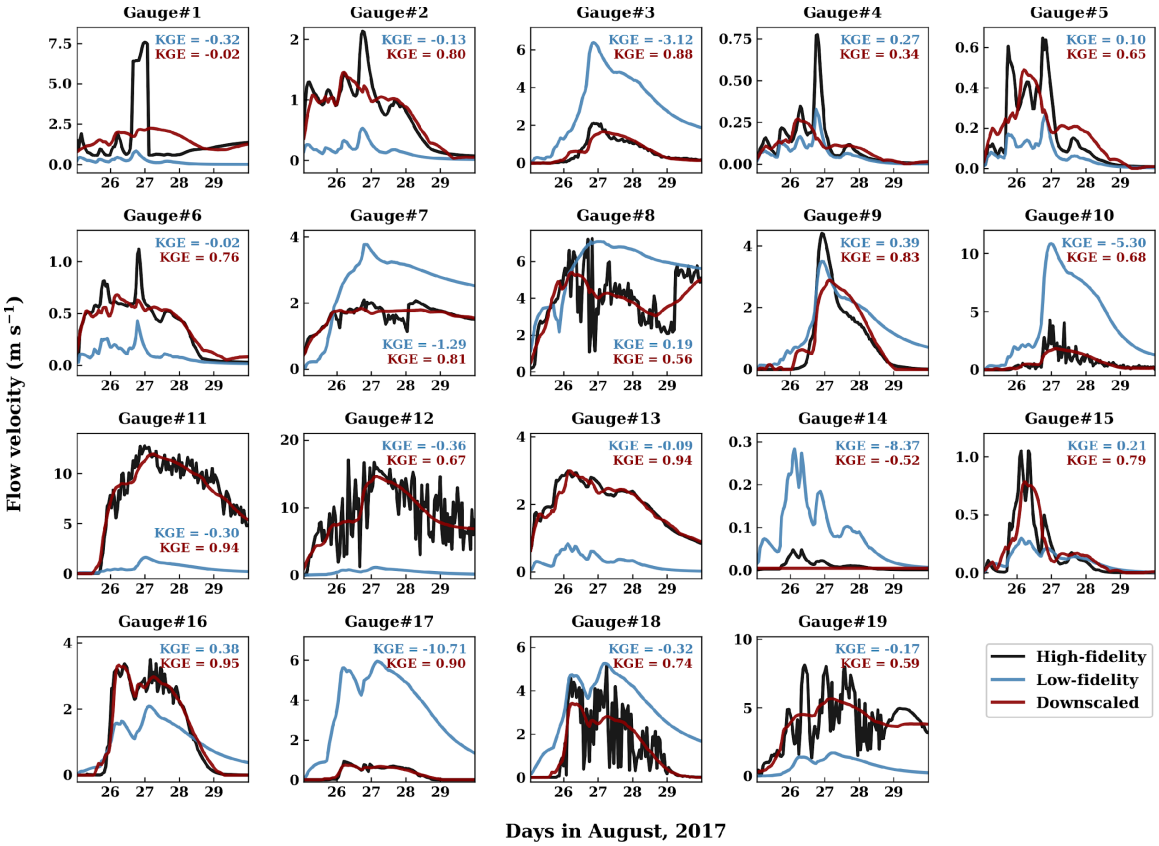

Figure S13. Comparison of the simulated flow velocity of the high-fidelity model, the low-fidelity model, and the downscaled model at the selected USGS gauges (see Table S1 and Figure 2b) during the Harvey flood event.

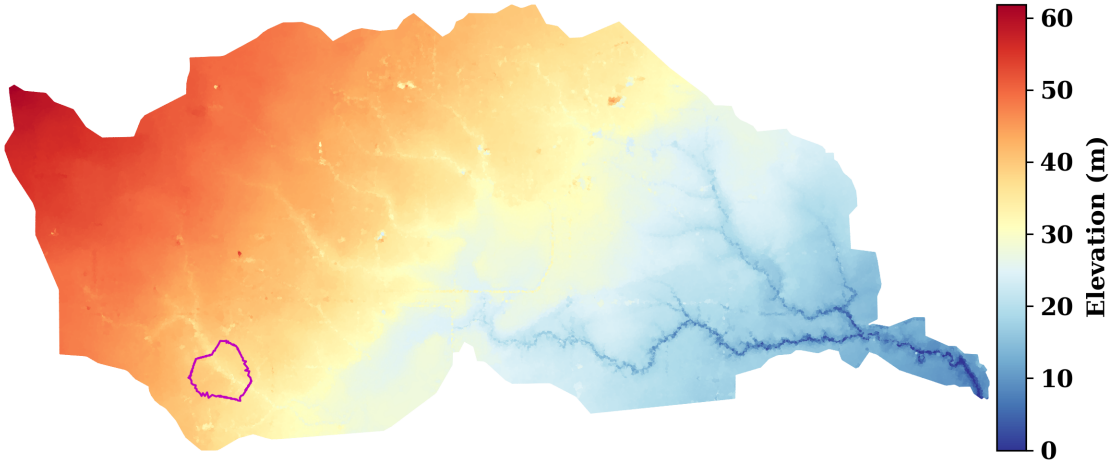

Figure S14. The area (circled in magenta) in the study domain selected for regionalized training of the LSG models for Gauge #1.